



1

2

3 **Variability of winter and summer surface ozone in Mexico City**
4 **on the intraseasonal time scale**

5

6

7

8

9 Bradford S. Barrett^{1,2} and Graciela B. Raga¹

10 ¹Centro de Ciencias de la Atmósfera, Universidad Nacional Autónoma de México, Mexico City 04510, Mexico

11 ²Oceanography Department, U.S. Naval Academy, Annapolis 21401, United States of America

12

13 *Correspondence to:* Graciela B. Raga (raga.graciela@gmail.com; raga@unam.mx)



14 **Abstract.** Surface ozone concentrations in Mexico City frequently exceed the Mexican standard
15 and have proven difficult to forecast due to changes in meteorological conditions at its tropical
16 location. The Madden-Julian Oscillation (MJO) is largely responsible for intraseasonal
17 variability in the tropics. Circulation patterns in the lower and upper troposphere and
18 precipitation are associated with the oscillation as it progresses eastward around the planet. It is
19 typically described by phases (labeled 1 through 8), which correspond to the broad longitudinal
20 location of the active component of the oscillation with enhanced precipitation. In this study we
21 evaluate the intraseasonal variability of winter and summer surface ozone concentrations in
22 Mexico City was investigated over the period 1986-2014 to determine if there is a modulation by
23 the MJO that would aid in the forecast of high pollution episodes.

24 Over 1 000 000 hourly observations of surface ozone from five stations around the metropolitan
25 area were standardized and then binned by active phase of the MJO, with phase determined using
26 the Real-time Multivariate MJO Index. Highest winter ozone concentrations were found in
27 Mexico City on days when the MJO was active and in phase 2 (over the Indian Ocean), and
28 highest summer ozone concentrations were found on days when the MJO was active and in
29 phase 6 (over the western Pacific Ocean). Lowest winter ozone concentrations were found during
30 active MJO phase 8 (over the eastern Pacific Ocean), and lowest summer ozone concentrations
31 were found during active MJO phase 1 (over the Atlantic Ocean). Anomalies of reanalysis-based
32 cloud cover and UV-B radiation supported the observed variability in surface ozone in both
33 summer and winter: MJO phases with highest ozone concentration had largest positive UV-B
34 radiation anomalies and lowest cloud cover fraction, while phases with lowest ozone
35 concentration had largest negative UV-B radiation anomalies and highest cloud cover fraction.
36 Furthermore, geopotential height anomalies at 250 hPa favoring reduced cloudiness, and thus



37 elevated surface ozone, were found in both seasons during MJO phases with above-normal ozone
38 concentrations. Similar height anomalies at 250 hPa favoring enhanced cloudiness, and thus
39 reduced surface ozone, were found in both seasons during MJO phases with below-normal ozone
40 concentrations. These anomalies confirm a physical pathway for MJO modulation of surface
41 ozone via modulation of the upper-troposphere.



42 **1 Introduction**

43 Ozone is hazardous to human health (WHO, 2008) and is a ubiquitous problem in many
44 megacities around the world. Tropospheric ozone is a secondary pollutant produced by complex
45 photochemistry from anthropogenic emissions and high ozone events typically affect mid-
46 latitude urban areas during summer, while in the tropics, such events can be observed throughout
47 the year. The problem of the incidence of high surface ozone events is exacerbated in Mexico
48 City, a megacity with 21 million inhabitants, because of the intense solar radiation received at its
49 relatively high elevation (more than 2200 m above sea level) and tropical latitude (19.4°N) (Lei
50 et al., 2007). Furthermore, the city is located in a basin, effectively preventing efficient
51 ventilation of the polluted air (Fast and Zhong, 1998; Whiteman et al., 2000; Zhang et al., 2009).

52 Seasonal variability in maximum surface ozone concentrations is not large in Mexico
53 City due to its geographical location (Raga and LeMoyne, 1996). Both in the dry winter
54 (December-February) and wet summer (June-August) months, clear skies and strong insolation
55 in the morning hours promote rapid generation of surface ozone via photochemical conversions
56 from anthropogenic precursor emissions near the surface. In both seasons, as the day progresses,
57 the boundary layer becomes unstable from solar radiation and deepens, diluting pollutant
58 concentrations near the surface. The growth of the boundary layer in Mexico City occurs over
59 the course of a few hours, with typical heights reaching at least 1.2 km above the surface
60 (Nickerson et al, 1992; Perez Vidal and Raga, 1998), even during the winter months when
61 insolation is reduced at this latitude. Highest ozone concentrations during the winter months are
62 often seen on days with strong insolation and light or no surface wind (Lei et al., 2007). In
63 summer months, clouds and precipitation generally reduce the number of days with extremely
64 elevated surface ozone concentrations. However, when large-scale atmospheric conditions are



65 favorable, such as when a high pressure regime and associated clear skies affect the Mexico City
66 basin, elevated concentrations of surface ozone are also recorded in summer (Raga and Le
67 Moyne, 1996). Hourly surface ozone concentrations routinely exceed the national standard, set
68 at 110 ppb in 1993 (by law NOM-020-SSA1-1993) and modified in 2014 to 95 ppb (by law
69 NOM-020-SSA1-2014). In 2015, hourly maximum O₃ concentrations in every month of the year
70 exceeded the standard set in 2014 at monitoring stations in all five geographic regions: NE, NW,
71 SE, SW and Center (Rodríguez et al., 2016).

72 The problem of air quality in Mexico City has been the subject of numerous field
73 programs over the years, typically limited in time but more comprehensive in terms of the
74 number of parameters measured. One such campaign was MILAGRO, a very large international
75 field campaign that took place in March 2006. The results of the large number of publications
76 from that project are summarized by Molina et al (2010). These results provided new insight into
77 several processes related with pollutant transformations and chemical pathways, emerging from
78 the analysis of the data collected with the large suite of sophisticated instrumentation deployed
79 and the modeling performed. However, intensive field campaigns limited to one month, cannot
80 address the seasonal and intraseasonal variability of the high surface ozone within the city.

81 Past studies have examined the variability of surface ozone in Mexico City at different
82 time scales, e.g. hourly (Raga and Le Moyne, 1996; Huerta et al., 2004; Lei et al., 2007), daily
83 (Fast and Zhong, 1998), weekly (Stephens et al., 2008), monthly (Rodríguez et al., 2016), and
84 seasonal (Thompson et al., 2008). All of these studies noted a primary relationship between
85 ozone concentration in Mexico City and ultraviolet (UV) radiation, where days with more UV
86 radiation were associated with elevated surface ozone concentrations. Furthermore, UV radiation
87 received at the surface is strongly modulated by cloud cover (El-Nouby Adam and Ahmed,



88 2016). However, as yet, no study has explored surface ozone variability in Mexico City on the
89 intraseasonal (30-60 day) time scale, despite known relationships between the leading mode of
90 atmospheric intraseasonal variability, the Madden-Julian Oscillation (MJO; Madden and Julian,
91 1971), and tropical cloud cover (Riley et al., 2011) and circulation (Madden and Julian, 1972;
92 Zhang, 2005). The MJO is largely responsible for intraseasonal variability in the tropics.
93 Circulation patterns in the lower and upper troposphere and precipitation are associated with the
94 oscillation as it progresses eastward around the planet. It is typically described by phases
95 (labeled 1 through 8), which correspond to the broad longitudinal location of the active
96 component of the oscillation with enhanced precipitation.

97 In this study we evaluate the intraseasonal variability of winter and summer surface
98 ozone concentrations in Mexico City over the period 1986-2014 to determine if there is a
99 modulation by the MJO that would aid in the forecast of high pollution episodes. Based on the
100 relationships between surface ozone and UV radiation, UV radiation and cloud cover, and cloud
101 cover and the MJO, the primary hypothesis tested in this study was the following: *surface ozone*
102 *varies intraseasonally by phase of the MJO.*

103 The physical pathway hypothesized to support this intraseasonal variability was as
104 follows: *anomalies in tropical convection associated with the MJO drive variability in upper*
105 *tropospheric circulation, and that variability can be seen in composite anomalies of height and*
106 *wind by MJO phase* (e.g., Madden and Julian, 1994; Zhang, 2005). Those circulation anomalies
107 then drive variability in cloud cover and thus variability in UV radiation reaching the boundary
108 layer, which in turn is seen in phase-to-phase variability in surface ozone concentrations in
109 Mexico City. The cloud-UV radiation portion of our hypothesis is supported by Kerr et al.
110 (2008), who found that typical UV transmission ratios range between 0.3 and 0.8 for overcast



111 conditions (Cede et al., 2002) and as little as 0.05 for thick cumulonimbus clouds (McArthur et
112 al., 1999). It is also supported by An et al. (2008), who found a strong relationship between
113 surface ozone concentrations in Beijing and surface UV radiation, particularly in summer, and
114 noted that surface UV was up to 200% more sensitive to total cloud cover than was surface total
115 radiation. The motivation to explore potential relationships between the MJO and surface ozone
116 concentrations came from Barrett et al. (2012), who found differences as large as 25% of the
117 daily mean in afternoon summer ozone concentrations in Santiago, Chile, by phase of the MJO
118 and tied those differences to changes in cloud fraction associated with synoptic-scale circulation
119 variability in different MJO phases.

120

121 **2 Data and methods**

122 The government monitoring network, Red Automática de Monitoreo Atmosférico
123 (Automated Atmospheric Monitoring Network, RAMA) has been operational since January 1986
124 measuring all criteria pollutants, with instrumentation certified by the US Environmental
125 Protection Agency (EPA). In particular, the instrument to measure ozone is produced by Thermo
126 Environmental Instrument Model 49, by UV absorbance. The RAMA currently has 33 stations
127 within the Mexico City basin, but only a few have records dating back to 1986.

128 We selected five stations with the longest periods of record (Table 1), one station from
129 each of the five geographic regions in the metropolitan area identified by several previous studies
130 and summarized by Raga et al. (2001). Hourly observations from Tlalnepantla (TLA, in the
131 NW), Xalostoc (XAL, in the NE), Merced (MER, in the Center), Pedregal (PED, in the SW), and
132 Universidad Autónoma Metropolitana-Iztapalapa (UIZ, in the SE) were available beginning in
133 January 1986 and up to December 2014. See Figure 1 for station locations and Table 1 for



134 numbers of observations and elevations of each station. Since the ozone time series were non-
135 stationary, standard anomalies (also called normalized anomalies) were calculated by subtracting
136 a mean value from each observation and then dividing that result by a standard deviation (Wilks,
137 2011). Those mean values and standard deviations for each hour were calculated on 30-day
138 (approximately monthly) basis, and the 30-day period was selected to avoid influence from both
139 seasonal variability and also the long-term trend. We did not stratify by day of the week based on
140 Stephens et al. (2008), who found that ozone in Mexico City exhibited relatively little variability
141 by day of the week. Furthermore, we defined a “low” ozone concentration day as one with mean
142 afternoon (1200 to 1600 local time) ozone standard anomalies (averaged across the five
143 observing stations) below the 10th percentile. Percentiles were determined separately for each
144 season using standard anomalies on all days in that season from 1986 to 2014. Similarly, we
145 defined a “high” ozone concentration day as one where mean afternoon ozone standard
146 anomalies exceeded the 90th percentile, again calculating winter and summer percentiles
147 separately.

148 The MJO phase was determined using the Real-time Multivariate MJO (RMM) index
149 (Wheeler and Hendon, 2004). The daily RMM is based on time series of two principal
150 components derived from empirical orthogonal functions of equatorially (5°S to 5°N) averaged
151 200-hPa zonal wind, 850-hPa zonal wind, and outgoing longwave radiation. The projection of
152 daily data onto the empirical orthogonal functions serves as a time filter and makes the RMM
153 useful in a real-time setting (Wheeler and Hendon, 2004). The RMM is divided into eight phases,
154 and each phase corresponds to the broad geographic location of the MJO tropical convective
155 signal on that day. An active MJO was defined in this study as one with RMM amplitude, which
156 is the square root of the sum of the squares of the two principal components RMM1 and RMM2



157 (Wheeler and Hendon, 2004), greater than 1.0 (LaFleur et al., 2015). Each day's hourly standard
158 ozone anomalies were binned using the phase of active MJO of that day. Mean values for each
159 MJO phase were then calculated, first annually and then for each season (DJF and JJA).

160 Values of geopotential height (in m) and u - and v vector wind components at 250 hPa (in
161 m s^{-1}), along with total cloud cover, high cloud cover, and low cloud cover (expressed as
162 fractions from 0 to 1) and downward UV radiation received at the surface (UV-B, in W m^{-2}) at
163 1800 UTC (1200 local time) were derived from the ERA-Interim reanalysis (Dee et al., 2011).
164 We chose to examine 250 hPa in part based on the results of Li et al. (2012), who connected
165 intraseasonal ozone variability across east Asia with variability in upper-troposphere
166 geopotential heights by MJO phase. Additionally, we are aware that cloud cover in reanalysis has
167 biases, and we selected the ERA-Interim product because it specifically includes an improved
168 deep convective cloud triggering mechanism over tropical land masses (Bechtold et al., 2004)
169 and thus shows skill over other products (Dee et al., 2011).

170 We selected the winter (Dec-Feb; DJF) and summer (June-August; JJA) seasons for this
171 study because of the homogeneity in synoptic-scale weather patterns in those seasons. More
172 details on the climatological variability of ozone in Mexico City can be found in Klaus et al.
173 (2001).

174 Finally, daily values of surface wind at the Tacubaya station (TCBY in Fig. 1) were taken
175 from the NOAA National Centers for Environmental Information (NCEI) Integrated Surface
176 Database (ISD; Smith et al., 2011). Anomalies of those values, calculated with respect to
177 seasonal means, were binned by MJO phase to give composite anomalies for each season. For
178 UV and total cloud cover in Mexico City itself, the gridded ERA-Interim value at the point
179 closest to the mean latitude and longitude of the five RAMA stations was selected.



180

181 **3 Results**182 **3.1 Variability of the ozone time series**

183 The diurnal cycle of ozone concentrations at each of the stations exhibited a daily
184 minimum around 0700 local time just prior to sunrise and a peak between 1200 and 1500 local
185 time, with highest concentrations at the southern-most stations (PED and UIZ) and lowest in the
186 northern-most station (XAL) (Fig. 2a). Additionally, highest ozone concentrations occurred one
187 to two hours earlier in spring (March-May; MAM) than in winter (December-February; DJF) at
188 both PED and XAL (Fig. 2b), and peak ozone at PED in the south occurred one to two hours
189 after peak ozone in XAL in the north, as a result of weak northeasterly surface winds
190 transporting ozone and photochemical precursors southward during the day (Bossert 1997).

191 Mean ozone concentrations in spring were nearly 30% higher at all stations than the rest
192 of the year (Fig. 3, with observations smoothed by a 30-day running mean), and the effects of
193 increased UV radiation during the “mid-summer drought” (*canícula*) (Magaña et al. 1999) were
194 reflected as a secondary peak in ozone concentrations in August. Minimum O₃ concentrations
195 were observed in all five stations during September, when daily maximum precipitation was
196 observed in Mexico City.

197 One of the challenges in examining intraseasonal variability of ozone is the need for a
198 stationary record over a long period. In Mexico City, ozone concentrations have steadily
199 decreased from the early 1990s to the 2010s (Fig. 4a; also Rodríguez et al., 2016) as a result of
200 pollution control measures (Molina and Molina, 2004). In order to remove the long-term trend,
201 while keeping the intraseasonal variability at hourly resolution, hourly observations were
202 converted to standard anomalies as described in Section 2. Results of this transformation of



203 hourly observations to standard anomalies for station PED are shown in Figures 4a (original
204 hourly observations) and 4c (hourly standard anomalies). Standard anomalies for the other four
205 stations show very similar results.

206 We note that overnight minimum observations from 1991 to 1993 were probably
207 overestimated in the observational record (Fig. 4a), an artifact also seen in the other four stations
208 (not shown). However, because in this study we focused on afternoon values (from 1200 to 1600
209 local time), that potential overestimation did not materially impact our results.

210 By transforming each hourly observation into a standard anomaly, the distribution of
211 relative frequencies shifted from highly non-Gaussian, with peaks near zero and very long right
212 tails (Fig. 4b), to more Gaussian, with peaks near -0.5 and reduced skewness (Fig. 4d). Although
213 the peaks in these transformed distributions were less than zero, and the right tails were longer
214 than the left tails, the means of each of the distributions of standard anomalies in Figure 4d were
215 very near zero, falling between -0.03 and 0.

216

217 **3.2 Synoptic patterns associated with low and high ozone**

218 Before examining ozone variability by MJO phase, it was important to first establish the
219 synoptic-scale patterns associated with days of low and high ozone concentrations (defined in
220 Section 2) in each season.

221 In winter (DJF), the synoptic pattern on days with low afternoon surface ozone
222 concentration featured a 250-hPa ridge over northwest Mexico and the southwest U.S. (height
223 anomalies up to +50 m) and a 250-hPa trough over central, eastern, and southern Mexico and the
224 southern and eastern U.S. (height anomalies -10 to -40 m) (Fig. 5a). Mean circulation at 250-hPa
225 on low DJF ozone days was nearly westerly off the central Mexican west coast turning to



226 southwesterly over central Mexico (Fig. 5a). This synoptic pattern would favor enhanced
227 cloudiness over Mexico City (and thus reduced UV radiation and lower ozone concentrations)
228 via two mechanisms: first, through quasi-geostrophic ascent associated with the 250-hPa trough,
229 and second, through advection of moisture and high-level clouds from the subtropical Pacific
230 (around 20°N) associated with westerly and west-northwesterly winds (Fig. 5a). Indeed, positive
231 total cloud fraction anomalies were seen with this height and circulation pattern, and those cloud
232 fraction anomalies (+0.05 to +0.10) extended over central and southern Mexico and
233 northeastward into the Gulf of Mexico (Fig. 5b). Those anomalies were likely comprised
234 primarily of high cloud (+0.05 to +0.15; Fig. 5c), given the resemblance between the pattern of
235 total cloud cover (Fig. 5b) and high cloud cover (Fig. 5c). A region of positive low cloud cover
236 anomalies (up to +0.15; Fig. 5d) was also seen in central Mexico on winter days with lowest O₃
237 concentrations, likely associated with surface wind convergence over the Sierra Madre Oriental
238 Mountains, although low cloud fraction anomalies over Mexico City itself were less than +0.05.

239 The synoptic pattern for winter days with high surface ozone concentration was opposite
240 that for the low ozone days. Over northwest Mexico and the southwest U.S., a trough was seen at
241 250-hPa (anomalies -10 to -70 m), while a ridge was seen over central, southern, and eastern
242 Mexico and the southern and eastern U.S. (anomalies to +50 m; Fig. 5e). Circulation at 250 hPa
243 over central Mexico was southwesterly (compared to westerly for low ozone days). Negative
244 total cloud fraction anomalies (-0.05 to -0.15) over central and southern Mexico were associated
245 with this circulation pattern (Fig. 5f). This pattern would promote clearer than normal skies (and
246 thus enhanced UV radiation and surface ozone production) by both favoring quasi-geostrophic
247 subsidence over central Mexico (associated with the above-normal heights and ridging at 250
248 hPa) and by advecting dry, cloud-free air toward central Mexico from the tropical East Pacific



249 Ocean originating near 10°N (Fig. 5g). Similar to low ozone days, most of the negative total
250 cloud fraction anomalies were likely result of the reduction in the presence of high cloud (Fig.
251 5g), given similarity of the anomaly patterns between total (Fig. 5f) and high (Fig. 5g) cloud
252 fraction. The low cloud fraction anomaly over Mexico City itself (Fig. 5h) was close to zero,
253 although negative low cloud fraction anomalies (-0.05 to -0.15) were seen over the low-land
254 states bordering the Gulf of Mexico (Fig. 5h).

255 Summer days with low surface ozone concentration featured a slight anomalous ridge
256 (height anomalies of +5 to +15 m) over northern Mexico and much of the U.S. (Fig. 6a). This
257 synoptic-scale pattern would favor cloudiness because positive geopotential height anomalies at
258 250 hPa over northern Mexico and the southwest U.S. would be associated with a stronger
259 summer anticyclone, signifying a more intense monsoon circulation, easterly winds at 250 hPa in
260 central and southern Mexico (Fig. 6a), and precipitation in central and southern Mexico. Indeed,
261 low ozone days featured positive anomalies in total cloud fraction (Fig. 6b), high cloud fraction
262 (Fig. 6c), and low cloud fraction (Fig. 6d), with anomalies of each fractional cloud cover variable
263 ranging from +0.05 to +0.15. The regions of positive total and high cloud cover anomalies
264 extended over much of central Mexico, but anomalies in low cloud fraction were confined to
265 Mexico City and the states bordering it (Fig. 6d). Summer days with high ozone concentration
266 featured less ridging over northwestern Mexico and the southwest U.S., with 250-hPa height
267 anomalies of -10 to -20 m (Fig. 6e). This synoptic-scale pattern with weaker ridging over
268 northwest Mexico and the southwest U.S., and stronger ridging over Central America, is
269 opposite of the climatological monsoon circulation and would favor less precipitation in central
270 Mexico. Indeed, negative anomalies in fraction of total cloud cover (Fig. 6f), high cloud cover
271 (Fig. 6g), and low cloud cover (Fig. 6h) were seen on days with high ozone concentrations, with



272 anomaly magnitudes of -0.05 to -0.15 over much of central and southern Mexico (total and high
273 cloud cover) and the states bordering Mexico City and along the Sierra Madre Occidental
274 mountains (Fig. 6h). In the next section, these seasonal ozone pattern composites are compared
275 to pattern composites for MJO phases with greatest ozone anomalies.

276

277 **3.3 Intraseasonal ozone variability**

278 On an annual basis, afternoon (1200 to 1600 local time) surface ozone concentrations in
279 Mexico City were found to vary by MJO phase. Highest ozone concentrations were noted on
280 days when MJO was active and in phases 3, 4, and 5, while lowest ozone concentrations were
281 noted on days when the MJO was active and in phases 1 and 2 (Fig. 7a). This variability was
282 seen at all five stations, regardless of geographic position within the basin. Normalized
283 anomalies of surface UV radiation and total cloud fraction from ERA-Interim reanalysis strongly
284 supported the observed surface ozone variability: MJO phases with highest ozone concentrations
285 also had highest UV anomalies and lowest total cloud fraction anomalies, while MJO phases
286 with lowest ozone concentrations had the most negative UV and the most positive cloud fraction
287 anomalies (Fig. 7d). We found this agreement remarkable, particularly so because the two data
288 sets independently presented the same intraseasonal pattern.

289 On a seasonal basis, surface ozone concentrations in Mexico City were also found to vary
290 by MJO phase. However, the dependence on phase was found to change between winter and
291 summer, meaning a phase associated with higher ozone concentrations in winter would not
292 necessarily be associated with higher ozone concentrations in summer. We attribute these
293 differences to seasonality in both the convective properties of the MJO itself (e.g., Zhang and
294 Dong, 2004; Wu et al., 2006) and in the extratropical atmosphere, whose circulation the MJO



295 modulates (Gloeckler and Roundy, 2013). Despite the phase-to-phase variability in maximum
296 and minimum ozone concentrations throughout the year, in all seasons, there remained good
297 agreement between phases with highest (lowest) ozone concentrations and phases with highest
298 (lowest) UV and lowest (highest) total cloud fraction. That is, the sunnier phases were
299 consistently associated with the highest ozone concentrations.

300 In winter months (DJF), highest ozone concentrations were found on days when the MJO
301 was in phase 2, and lowest ozone concentrations were found on days when the MJO was in phase
302 8 (Fig. 7b). Highest UV radiation, and lowest total cloud fraction, were seen on days when the
303 MJO was in phase 2, and lowest UV radiation and second-highest cloud fraction were seen on
304 days when the MJO was in phase 8 (Fig. 7e). In summer months (JJA), highest ozone
305 concentrations were found on days when the MJO was in phases 5, 6, and 7, and lowest ozone
306 concentrations were found on days when the MJO was in phases 1 and 8 (Fig. 7c). Highest UV
307 radiation, and lowest total cloud fraction, was seen on days when the MJO was in phase 6, and
308 lowest UV radiation and highest total cloud fraction were seen on days when the MJO was in
309 phase 1. In both winter and summer, UV radiation and cloud cover anomalies strongly supported
310 observed surface ozone anomalies, whereby the cloudiest MJO phases featured lowest ozone and
311 the sunniest phases featured highest ozone. We again consider this agreement remarkable, given
312 the independence of the ozone and reanalysis data sets. Summer months (JJA) featured the
313 greatest range in mean ozone concentrations by MJO phase: a difference in 0.25 standard
314 anomaly units between the phases with the highest ozone concentrations (phases 5 and 6) and the
315 phases with the lowest ozone concentrations (phases 1 and 8) (Fig. 7c). Summer months also
316 featured the largest spread in both UV and total cloud fraction standard anomalies (Fig. 7f).



317 An examination of the frequency of “extreme” ozone days in each MJO phase (here a day
318 with an “extreme” ozone value was defined for each season as an afternoon standard anomaly
319 either above the 90th percentile value or below the 10th percentile value) provides additional
320 insight into the character of the MJO modulation of ozone. In both winter and summer, the
321 phases associated with highest ozone concentrations (phase 2 in winter and phase 6 in summer)
322 featured the fewest occurrences of days with extremely low ozone (days with concentrations
323 below the 10th percentile; Table 2). Those phases also featured either the highest (in summer) or
324 near-highest (in winter) occurrences of days with concentrations above the 90th percentile (Table
325 2). Furthermore, the phases associated with lowest ozone concentration (phase 8 in winter and
326 phase 1 in summer) featured the highest occurrences of days with low ozone (Table 2) and
327 below-normal occurrence of days with high ozone. These results confirm that one manner in
328 which the MJO modulates ozone concentration in Mexico City is to reduce (or augment) the
329 frequency of days with afternoon ozone concentrations either below the 10th or above the 90th
330 percentiles.

331 To examine physical mechanisms for the observed variability in ozone concentration and
332 cloud cover by MJO phase, composite anomalies of 250-hPa height and *u*- and *v*- wind
333 components were created for each active MJO phase for each season. Seasonal anomalies of total
334 cloud fraction, high cloud fraction, and low cloud fraction were also composited for each active
335 MJO phase. In both seasons, anomalies of each variable were found for all eight MJO phases.
336 However, for the remainder of this paper, we focus only on the synoptic-scale conditions in
337 phases with maximum and minimum surface ozone. In DJF, minimum ozone concentrations
338 occurred on days when the MJO was active and in phase 8. In that phase, anomalous 250-hPa
339 ridging was seen over northwest Mexico and the southwest U.S. (anomalies up to +50 m) and



340 anomalous 250-hPa troughing over northeast Mexico and the southeastern U.S. (anomalies to -60
341 m) (Fig. 8a). This height pattern resembled the seasonal pattern for winter days with above-
342 normal cloudiness and low ozone (Figs. 5a), with troughing over central Mexico favoring both
343 cloud formation via ascent and cloud advection from the subtropical East Pacific Ocean. Indeed,
344 on days in MJO phase 8, total cloud cover anomalies were positive over nearly all of Mexico,
345 ranging from +0.05 to +0.15 (Fig. 8b). Anomalies in high cloud cover were smaller in magnitude
346 (up to +0.05), and over Mexico City, high cloud cover anomalies were zero (Fig. 8c). Positive
347 low cloud anomalies were confined to the states to the east of Mexico City (Fig. 8d), which when
348 combined with high cloud cover anomalies, suggest that the anomalies in total cloud cover (Fig.
349 8b) were composed of anomalies at multiple levels.

350 Maximum winter ozone concentrations occurred on days when the MJO was active and
351 in phase 2, and on those days, a synoptic-scale pattern opposite to that of phase 8 was seen:
352 anomalous 250-hPa troughing was seen over northern Mexico and the south-central U.S. (height
353 anomalies of -10 to -30 m) and anomalous 250-hPa ridging was seen over central and southern
354 Mexico and Central America (height anomalies +5 to +20 m) (Fig. 8e). This height pattern
355 resembled the seasonal pattern for high ozone and low cloud fraction (Fig. 5e), with anomalous
356 ridging favoring clearer than normal skies via subsidence and advection of dry air from the
357 tropical East Pacific. Indeed, below-normal total cloud fraction (anomalies -0.05 to -0.15; Fig.
358 8f), high cloud fraction (anomalies -0.05 to -0.15; Fig. 8g), and low cloud fraction (anomalies -
359 0.05 to -0.10; Fig. 8h) were seen on days when the MJO was in phase 2 over much of central and
360 southern Mexico.

361 In JJA, minimum ozone concentrations occurred on days when the MJO was in phase 1.
362 In that phase, anomalous 250-hPa ridging was seen over northwest Mexico and the southwest



363 U.S. (anomalies up to +20 m) and anomalous 250-hPa troughing in the tropical East Pacific
364 Ocean (anomalies to -20 m) (Fig. 9a). This height pattern resembled the seasonal pattern for
365 summer days associated with below-normal cloudiness and high ozone (Figs. 6a), with ridging to
366 the north characteristic of the summer monsoon in central Mexico. Indeed, above-normal total
367 cloud fraction (+0.05 to +0.15; Fig. 9b), above-normal high cloud fraction (+0.05 to +0.15; Fig.
368 9c), and above-normal low cloud fraction (+0.05 to +0.10; Fig. 9d) were seen over central and
369 southern Mexico for days in MJO phase 1. Summer maximum ozone concentrations were seen
370 on days when the MJO was in phase 6. In that phase, a weaker-than-normal ridge at 250 hPa was
371 seen as anomalous heights of -10 to -20 m over much of central Mexico (Fig. 9e). This height
372 pattern resembled the seasonal pattern for summer days associated with above-normal cloudiness
373 and high ozone (Figs. 6e), as it is largely opposite of that which characterizes the central Mexico
374 summer monsoon. Indeed, below-normal total cloud fraction (-0.05 to -0.15; Fig. 9f), high cloud
375 fraction (-0.05 to -0.15; Fig. 9g), and low cloud fraction (-0.05; Fig. 9h) were all seen on days
376 when the MJO was in phase 6.

377 The final physical variable examined for intraseasonal variability by MJO phase was the
378 surface wind vector at 1800 UTC (1200 local time) at Tacubaya (TCBY in Fig. 1) in the center-
379 west portion of the metropolitan area (Fig. 1). In winter, days in phase 8 (lowest ozone
380 concentrations) featured anomalous westerly surface winds (blue vectors; Fig. 10), resulting in
381 observed wind speeds up to 50% weaker than climatology (red vectors in Fig. 10). Days in phase
382 2 (highest ozone concentrations) featured small or weakly anomalous easterly winds, resulting in
383 winds similar to climatology but up to 40% stronger in magnitude (Fig. 10). In summer, days in
384 phases 8 and 1 (lowest ozone concentrations) featured surface winds very similar to climatology
385 in both magnitude and direction. In summer, the wind direction on days in phase 8 was more



386 from the north-northwest, while climatology was from the north-northeast. Days in phase 6
387 (highest ozone concentrations) also featured winds with similar direction as the seasonal mean,
388 but with speeds up to 30% faster (Fig. 10). Despite these variations by MJO phase across all
389 seasons, we do not consider the surface wind anomalies to be physically consistent or
390 representative of a large scale pattern, for two reasons. First, because Mexico City is located in a
391 basin, surface flow fields do not normally respond to synoptic-scale pattern variability (Stephens
392 et al., 2008). Indeed, the majority of the day-to-day variability in surface wind speed and
393 direction is controlled by mesoscale, thermally-driven mountain-valley circulations (Doran et al.,
394 1998). With the exception of “cold surge” events in winter that have been associated with cloudy
395 days, the two dominant ozone patterns identified by De Foy et al. (2005) only served to identify
396 whether the ozone maximum would be in the southern or northern parts of the metropolitan area.
397 Second, the wind anomalies by MJO phase resulted in only subtle changes in either direction, or
398 speed, or both (Fig. 10). Moreover, none of the wind anomalies identified in DJF would meet the
399 northerly “cold surge” of De Foy et al. (2005), suggesting that the “cold surge” events can occur
400 during different MJO phases unrelated to modulation from the MJO. Finally, the smallness of the
401 surface wind variability by MJO phase supports our argument that variability in surface ozone
402 concentrations by MJO phase are primarily driven by variability in total cloud cover and surface
403 UV radiation, which in turn are related to anomalies in upper-tropospheric circulation.

404

405 **4 Conclusions**

406 In this study, we investigated the intraseasonal variability of winter (DJF) and summer
407 (JJA) surface ozone concentrations in Mexico City. After standardizing over 1 000 000 hourly
408 observations of surface ozone from five stations around the metropolitan area, we binned them



409 by phase of the active MJO. We found that highest winter ozone concentrations occurred on days
410 when the MJO was active and in phase 2 (in the Indian Ocean), and highest summer ozone
411 concentrations occurred on days when the MJO was active and in phase 6 (in the western Pacific
412 Ocean) in summer. Lowest ozone concentrations were found on winter days in MJO phase 8 (in
413 the eastern Pacific Ocean) and summer phase 1 (in the Atlantic Ocean). This intraseasonal
414 variability in surface ozone concentrations agreed well with anomalies in cloud cover and UV-B
415 radiation: phases with highest ozone concentration had highest UV-B radiation and lowest cloud
416 cover, while phases with lowest ozone concentration had lowest UV-B radiation and highest
417 cloud cover. This agreement was found for both winter and summer. Circulation anomalies at
418 250 hPa were found to support the observed variability in ozone and cloud cover. In winter,
419 height and circulation anomalies favoring reduced cloudiness, and thus elevated surface ozone,
420 were found on days when the MJO was in phase 2, and height and circulation anomalies favoring
421 enhanced cloudiness, and thus reduced surface ozone, were found on days when the MJO was in
422 phase 8. In summer, monsoon-like 250-hPa circulation patterns that favor enhanced cloudiness,
423 and thus reduced surface ozone, were found on days when the MJO was in phase 1, and 250-hPa
424 circulation patterns opposite to the monsoon, favoring reduced cloudiness and thus elevated
425 surface ozone, were found on days when the MJO was in phase 6. We did not find physically
426 meaningful variability in surface wind direction by MJO phase, despite earlier studies suggesting
427 a relationship between surface wind and surface ozone in Mexico City. This suggests that the
428 intraseasonal variability in both summer and winter surface ozone by MJO phase is driven
429 primarily by variability in cloud cover via modulation of upper-troposphere circulation.

430

431



432 *Acknowledgements*

433 Partial funding for B. Barrett was provided by the Fulbright Scholar program of the U.S.
434 State Department and the Programa de Estancias de Investigación, Dirección General de
435 Personal Académico, Universidad Nacional Autónoma de México (DGAPA-UNAM). The air
436 quality data were obtained from the databases of the Mexico City's Air Quality Monitoring
437 Network operated by the Ministry of Environment of Mexico City. ERA-Interim data were
438 provided courtesy of ECMWF.



439 **References**

- 440 An, J. L., Wang, Y. S., Li, X., Sun, Y., and Shen, S H.: Relationship between surface UV
441 radiation and air pollution in Beijing (in Chinese). *Environ. Sci*, 29, 1054-1058, 2008.
- 442 Barrett, B. S., Fitzmaurice, S. J., and Pritchard S. R.: Intraseasonal variability of surface ozone in
443 Santiago, Chile: modulation by phase of the Madden-Julian Oscillation (MJO). *Atmos.*
444 *Environ.*, 55, 55-62, 2012.
- 445 Bechtold, P., Chaboureaud, J. P., Beljaars, A. C. M., Betts, A. K., Kohler, M., Miller, M.,
446 Redelsperger, J.-L.: The simulation of the diurnal cycle of convective precipitation over
447 land in a global model. *Q. J. R. Meteorol. Soc.*, 130, 3119–3137, 2004.
- 448 Bossert, J. E.: An investigation of flow regimes affecting the Mexico City Region. *J. Applied*
449 *Meteor.*, 36(2), 119-140, 1997.
- 450 Cede, A., Blumthaler, M., Luccini, E., Piacentini, R. D., and Numez, L.: Effects of clouds on
451 erythemal and total irradiance as derived from data of the Argentine Network. *Geophys.*
452 *Res. Lett.*, 29, doi:10.1029/2002GL015708, 2002.
- 453 Dee, D. P., and Co-authors: The ERA-Interim reanalysis: configuration and performance of the
454 data assimilation system. *Q. J. R. Meteorol. Soc.*, 137, 553-597, 2011.
- 455 De Foy, B., Caetano, E., Magaña, V., Zitácuaro, A., Cárdenas, B., Retama, A., Ramos, R.,
456 Molina, L. T., and Molina, M. J.: Mexico City basin wind circulation during the MCMA-
457 2003 field campaign. *Atmos. Chem. Phys.*, 5, 2267-2288, 2005.
- 458 Doran, J. C., Abbot, S., Archuleta, J., and Bian, X.: The IMADA-AVER boundary layer
459 experiment in the Mexico City area. *Bull. Amer. Meteor. Soc.*, 79, 2497-2508, 1998.



- 460 El-Nouby Adam, M. and Ahmed, E. A.: An assessment of the ratio of ultraviolet-B to broadband
461 solar radiation under all cloud conditions at a subtropical location. *Adv. Space Res.*,
462 57(3), 764-775, 2016.
- 463 Fast, J. D. and Zhong, S.: Meteorological factors associated with inhomogeneous ozone
464 concentrations within the Mexico City basin. *J. Geophys. Res.*, 103(D15), 18927-18946,
465 1998.
- 466 Gloeckler, L. C. and Roundy, P. E.: Modulation of the extratropical circulation by combined
467 activity of the Madden-Julian Oscillation and equatorial Rossby waves during boreal
468 winter. *Mon. Wea. Rev.*, 141, 1347-1357, 2013.
- 469 Huerta, G., Sansó, B., and Stroud, J. R.: A spatiotemporal model for Mexico City ozone levels.
470 *Appl. Statist.*, 53(2), 231-248, 2004.
- 471 Kerr, J. B., and Fioletov, V. E.: Surface ultraviolet radiation. *Atmos.-Ocean*, 46, 159-184, 2008.
- 472 Klaus, D., Poth, A., Voss, M. and Jáuregui, E.: Ozone distributions in Mexico City using
473 principal component analysis and its relation to meteorological parameters. *Atmósfera*,
474 14(4), 171-188, 2001.
- 475 LaFleur, D. M., Barrett, B. S., and Henderson, G. R.: Some climatological aspects of the
476 Madden-Julian Oscillation (MJO). *J. Climate*, 28, 6039-6053, 2015.
- 477 Lei, W., de Foy, B., Zavala, M., Volkamer, R., and Molina, L. T.: Characterizing ozone
478 production in the Mexico City Metropolitan Area: a case study using a chemical transport
479 model. *Atmos. Chem. Phys.*, 7, 1347-1366, 2007.
- 480 Li, K.-F., Tian, B., Waliser, D. E., Schwartz, M. J., Neu, J. L., Worden, J. R., and Yung, Y. L.:
481 Vertical structure of MJO-related subtropical ozone variations from MLS, TES, and
482 SHADOZ data. *Atmos. Chem. Phys.*, 12, 425-436, 2012.



- 483 Madden, R. and Julian, P.: Detection of a 40-50 day oscillation in the zonal wind in the tropical
484 Pacific, *J. Atmos. Sci.*, 28, 702-708, 1971.
- 485 Madden, R. and Julian, P.: Description of global-scale circulation cells in the tropics with a 40-
486 50 day period. *J. Atmos. Sci.*, 29, 1109-1123, 1972.
- 487 Madden, R. and Julian, P.: Observations of the 40-50 day tropical oscillation: a review. *Mon.*
488 *Wea. Rev.*, 122, 814-837, 1994.
- 489 Magaña, V., Amador, J. A., and Medina, S.: The midsummer drought over Mexico and Central
490 America. *J. Climate*, 12(6), 1577-1588, 1999.
- 491 McArthur, L. J. B., Fioletov, V. E., Kerr, J. B., McElroy, C. T., and Wardle, D. I. Derivation of
492 UV-A irradiance from pyranometer measurements. *J. Geophys. Res.*, 104, 1999.
- 493 Molina, L. T., S. Madronich, J. S. Gaffney, E. Apel, B. de Foy, J. Fast, R. Ferrare, S. Herndon, J.
494 L. Jimenez, B. Lamb, A. R. Osornio-Vargas, P. Russell, J. J. Schauer, P. S. Stevens, R.
495 Volkamer, and M. Zavala: An overview of the MILAGRO 2006 Campaign: Mexico City
496 emissions and their transport and transformation. *Atmos. Chem. Phys.*, 10, 8697-8760,
497 2010.
- 498 Molina, L. T. and Molina, M. J.: Improving air quality in megacities: Mexico City case study.
499 *Annals of the New York Acad. Sci.*, 1023, 142-158, 2004.
- 500 Nickerson, C. E., Sosa, G., Hochstein, H., MacCaslin, P., Luke, W., and Schanot, A.:
501 Measurements of Mexico City air pollution by a research aircraft. *Atmos. Environ.*, 26B,
502 445-451, 1992.
- 503 Perez Vidal, H. and Raga, G. B.: On the vertical distribution of pollutants in Mexico City.
504 *Atmósfera*, 11, 95-108, 1998.



- 505 Raga, G. B. and Le Moyne, L.: On the nature of air pollution dynamics in Mexico City—I.
506 Nonlinear analysis. *Atmos. Environ.*, 30(23), 3987-3993, 1996.
- 507 Raga, G. B., Baumgardner, D., Castro, T., Martinez-Arroyo, A., and Navarro-Gonzalez, R.:
508 Mexico City air quality: A qualitative review of gas and aerosol measurements (1960-
509 2000). *Atmos. Environ.*, 35, 4041-4058, 2001.
- 510 Riley, E. M., Mapes, B. E., and Tulich, S. N.: Clouds associated with the Madden-Julian
511 Oscillation: a new perspective from CloudSat. *J. Atmos. Sci.*, 68, 3032-3061, 2011.
- 512 Rodríguez, S., Huerta, G., and Reyes, H.: A study of trends for Mexico City ozone extremes:
513 2001-2014. *Atmósfera*, 29(2), 107-120, 2016.
- 514 Smith, A., Lott, N., and Vose, R.: The Integrated Surface Database: Recent Developments and
515 Partnerships. *Bull. Amer. Meteor. Soc.*, 92, 704–708, 2011.
- 516 Stephens, S., Madronich, S., Wu, F., Olson, J. B., Ramos, R., Retama, A., and Muñoz, R.:
517 Weekly patterns of México City’s surface ozone concentrations of CO, NO_x, PM₁₀ and
518 O₃ during 1986-2007. *Atmos. Chem. Phys.*, 8, 5313-5325, 2008.
- 519 Thompson, A. M., Yorks, J. E., Miller, S. K., Witte, J. C., Dougherty, K. M., Morris, G. A.,
520 Baumgardner, D., Ladino, L., and Rappenglück, B.: Tropospheric ozone sources and
521 wave activity over Mexico City and Houston during MILAGRO/Intercontinental
522 Transport Experiment (INTEX-B) Ozonesonde Network Study, 2006 (IONS-06). *Atmos.*
523 *Chem. Phys.*, 8, 5113-5125, 2008.
- 524 Wilks, D., 2011: *Statistical Methods in the Atmospheric Sciences*. Academic Press, 3rd ed., 704
525 pp.



- 526 Whiteman, C.D., Zhong, S., Bian, X., Fast, J.D., Doran, J.C.: Boundary layer evolution and
527 regional-scale diurnal circulations over the Mexico Basin and Mexican Plateau. *J.*
528 *Geophys Res* 105, 10081-10102, 2000.
- 529 WHO: Health risks of ozone from long-range transboundary air pollution. World Health
530 Organization, 2008. [available on-line at [http://www.euro.who.int/__data/assets/pdf_file/](http://www.euro.who.int/__data/assets/pdf_file/0005/78647/E91843.pdf)
531 [0005/78647/E91843.pdf](http://www.euro.who.int/__data/assets/pdf_file/0005/78647/E91843.pdf)].
- 532 Wu, M.-L. C., Schubert, S. D., Suarez, M. J., Pegion, P. J., and Waliser, D. E.: Seasonality and
533 meridional propagation of the MJO. *J. Climate*, 19, 1901-1921, 2006.
- 534 Zhang, C. Madden-Julian Oscillation. *Rev. Geophys.*, 43, 1-36, 2005.
- 535 Zhang, C., and Dong, M.: Seasonality in the Madden-Julian Oscillation. *J. Climate*, 17, 3169-
536 3180, 2004.
- 537 Zhang, Y., Dubey, M. K., Olsen, S. C., Zheng, J., and Zhang, R.: Comparisons of WRF/Chem
538 simulations in Mexico City with ground-based RAMA measurements during the 2006-
539 MILAGRO campaign. *Atmos. Chem. Phys.*, 9, 3777-3798, 2009.



540 **Table captions**

541 Table 1: Station names, locations, period of record, and number of observations.

542

543 Table 2: Relative frequency of extreme ozone days in winter (top two rows) and summer (bottom
544 two rows). An extreme ozone day was defined as one with mean afternoon hourly (1200 to 1600
545 local) ozone concentrations at average of all 5 stations either greater than the 90th percentile
546 value or less than the 10th percentile value. Bold values (winter phase 2; summer phase 6)
547 indicate phases with highest mean ozone concentrations in those seasons; values in italics (winter
548 phase 8; summer phase 1) indicate phases with lowest mean ozone concentrations in those
549 seasons. Number of days (n) in each active phase is given for each season.

550

551

552 **Figure captions**

553 Figure 1: Locations of RAMA surface ozone stations used in this study (colored dots;
554 abbreviations defined in Table 1) and topographic height (shaded, in m) of the Mexico City
555 metropolitan region. State boundaries shown as black contours. Surface meteorology station at
556 Tacubaya (TCBY) also indicated. The inset in the upper right corner shows the location of
557 Mexico City within Mexico.

558

559 Figure 2: (a) Diurnal cycle of surface ozone concentrations (ppb) at five observing stations
560 (colored lines), as well as the mean (black dotted line) for all seasons, 1986-2014. (b) Diurnal
561 cycle of surface ozone concentrations for Pedregal (PED; blue lines) and Xalostoc (XAL; red
562 lines) by season from the RAMA network, 1986-2014.



563 Figure 3: Annual cycles of surface ozone concentrations (ppb) for five observing stations for
564 hours 1200-1600 (local time) from the RAMA network, 1986-2014. Observations are smoothed
565 using a 30-day running mean.

566

567 Figure 4: (a) Hourly observations of surface ozone concentrations (ppb) at Pedregal station (PED
568 in Fig. 1). (b) Relative frequencies (in %) of hourly ozone concentrations (ppb) at five observing
569 stations, 1986-2014. (c) Standard anomalies of hourly surface ozone concentrations at PED. (d)
570 Relative frequencies (in %) of standard anomalies of hourly ozone concentrations at five
571 observing stations from the RAMA network, 1986-2014.

572

573 Figure 5: (a) Height (contoured, in m), height anomalies (shaded, in m), and mean winds
574 (vectors) at 250-hPa for winter (DJF) days with standard anomalies of afternoon (1200 to 1600
575 local time) surface ozone at the five observing stations (Fig. 1) below the 10th percentile. (b)-(d)
576 Anomalies (in %) of total cloud fraction, high cloud fraction, and low cloud fraction,
577 respectively, for the same winter days with standard anomalies of afternoon surface ozone
578 concentrations below the 10th percentile. (e)-(h) Same as in (a)-(d), but for winter days with
579 mean afternoon surface ozone concentrations above the 90th percentile. Percentile calculations
580 based on hourly observations from 1986-2014. Height, wind, and cloud fraction data from ERA-
581 Interim; ozone concentrations from RAMA stations.

582

583 Figure 6: As in Figure 5, but for summer (JJA) days.

584



585 Figure 7: Mean standard anomalies of midday (hours 12-16 local time) surface ozone
586 concentrations by active MJO phase for (a) annual, (b) DJF, and (c) JJA. Stations indicated by
587 line color. Error bars indicate largest and smallest standard anomaly values for all stations;
588 dashed black curve indicates mean value. All surface ozone observations from the RAMA
589 network, 1986-2014. (d) Standard anomalies of UV radiation (blue curves) and total cloud
590 fraction (black curves) for each active MJO phase for the entire year. (e) and (f) Same as panel
591 (d) but for DJF and JJA, respectively. UV and cloud fraction data from ERA-Interim reanalysis,
592 1986-2014, for the grid closest to Mexico City.

593

594 Figure 8: Composites of 250-hPa height (in m), height anomaly (in m), and mean wind (a), and
595 total cloud fraction (in %; b), high cloud fraction (in %; c), and low cloud fraction (in %; d) for
596 winter days in active MJO phase 8. (e)-(h) Same as (a)-(d) but for winter days in active MJO
597 phase 2. Phases 8 and 2 were the phases with lowest and highest respective winter ozone
598 concentrations in Mexico City.

599

600 Figure 9: As in Figure 8, but for summer days in active MJO phase 1 (a-d) and active MJO phase
601 6 (e-h). Phases 1 and 6 were the phases with lowest and highest respective summer ozone
602 concentrations in Mexico City.

603

604 Figure 10: Mean 10-m winds at Tacubaya station (TCBY in Fig. 1) at 1800 UTC (1200 local
605 time). Mean surface wind vectors for each season, DJF and JJA, are on row one and indicated by
606 red arrows. Mean (black arrows) and anomaly (blue arrows) vectors for the MJO phases
607 associated with lowest surface ozone (phase 8 in DJF and phase 1 in JJA) are on the middle row.



608 Mean (black arrows) and anomaly (blue arrows) vectors for the MJO phases associated with
609 highest surface ozone (phase 2 in DJF and phase 6 in JJA) are on the bottom row. Note that the
610 mean winds for low ozone in DJF and high ozone in JJA are very similar to the seasonal mean
611 winds, so the anomaly (blue) vector is very small. All wind data are from NOAA National
612 Centers from Environmental Information, 1986-2014.



Table 1: Station names, locations, period of record, and number and type of observations.

Station name	Abbreviation	Latitude (°N)	Longitude (°W)	Elevation (m)	Period of record	Variable	Number of observations	Frequency of observation
Xalostoc	XAL	19.3	-99.2	2326	1986 to 2014	Surface O ₃	221472	Hourly
Tlalnepantla	TLA	19.4	-99.1	2245	1986 to 2014	Surface O ₃	230992	Hourly
Merced	MER	19.5	-99.1	2160	1986 to 2014	Surface O ₃	219404	Hourly
Pedregal	PED	19.5	-99.2	2311	1986 to 2014	Surface O ₃	217009	Hourly
UAM-Iztapalapa	UIZ	19.4	-99.1	2221	1986 to 2014	Surface O ₃	194224	Hourly
Tacubaya	TCBY	19.4	-99.2	2313	1986 to 2014	Surface wind	7398	Daily (at 1200 local)

613

614



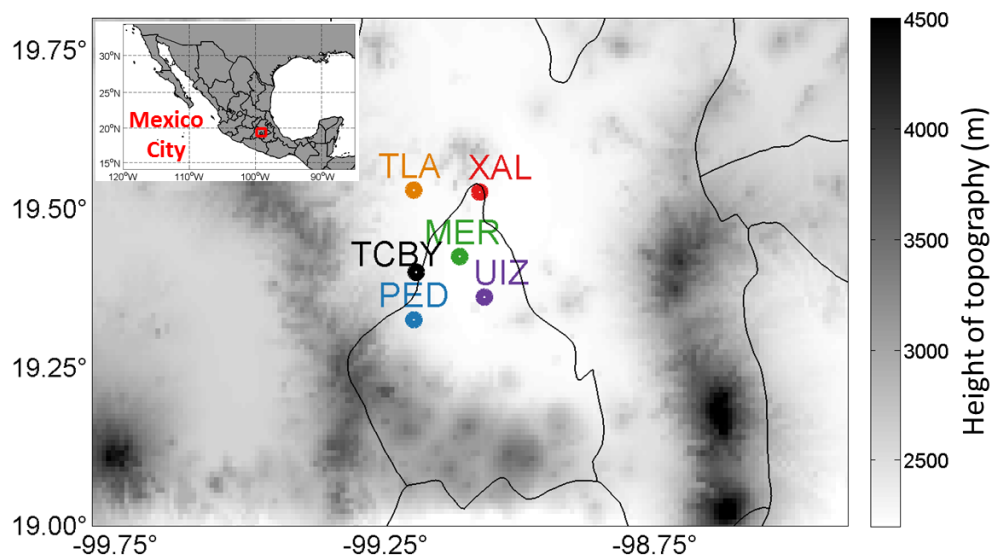
Table 2: Relative frequency of extreme ozone days in winter (top two rows) and summer (bottom two rows). An extreme ozone day was defined as one with mean afternoon hourly (1200 to 1600 local) ozone concentrations at average of all 5 stations either greater than the 90th percentile value or less than the 10th percentile value. Bold values (winter phase 2; summer phase 6) indicate phases with highest mean O₃ concentrations in those seasons; italics values (winter phase 8; summer phase 1) indicate phases with lowest mean O₃ concentrations in those seasons. Number of days (n) in each active phase is given for each season.

	Phase 1	Phase 2	Phase 3	Phase 4	Phase 5	Phase 6	Phase 7	Phase 8
Winter (DJF)	n=134	n=169	n=249	n=222	n=226	n=254	n=282	n=187
Relative frequency of days with O ₃ concentration greater than the 90th percentile	9.7%	10.1%	7.6%	8.1%	12.8%	9.8%	12.4%	<i>8.6%</i>
Relative frequency of days with O ₃ concentration less than the 10th percentile	9.0%	7.1%	7.2%	8.1%	7.5%	9.8%	12.4%	<i>13.9%</i>
Summer (JJA)	n=351	n=267	n=112	n=114	n=165	n=137	n=121	n=161
Relative frequency of days with O ₃ concentration greater than the 90th percentile	<i>8.6%</i>	6.7%	3.6%	10.5%	9.7%	11.7%	11.6%	8.7%
Relative frequency of days with O ₃ concentration less than the 10th percentile	<i>17.1%</i>	9.0%	10.7%	4.4%	5.5%	3.7%	9.1%	14.9%

615

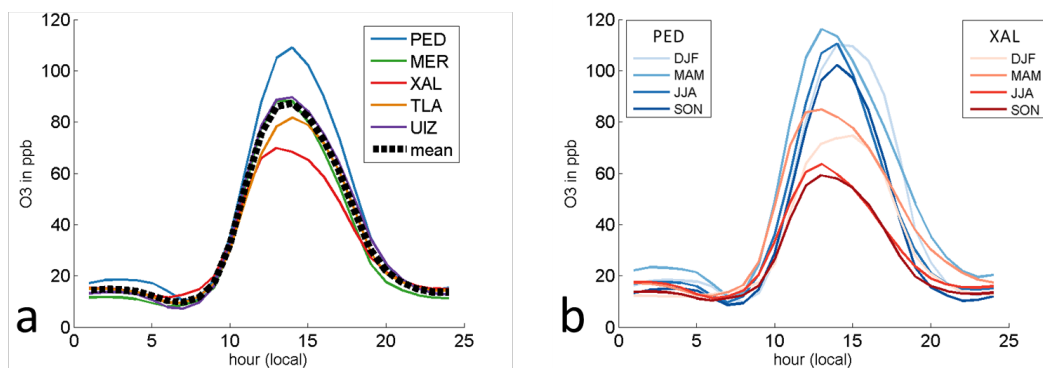


616 **Figures**



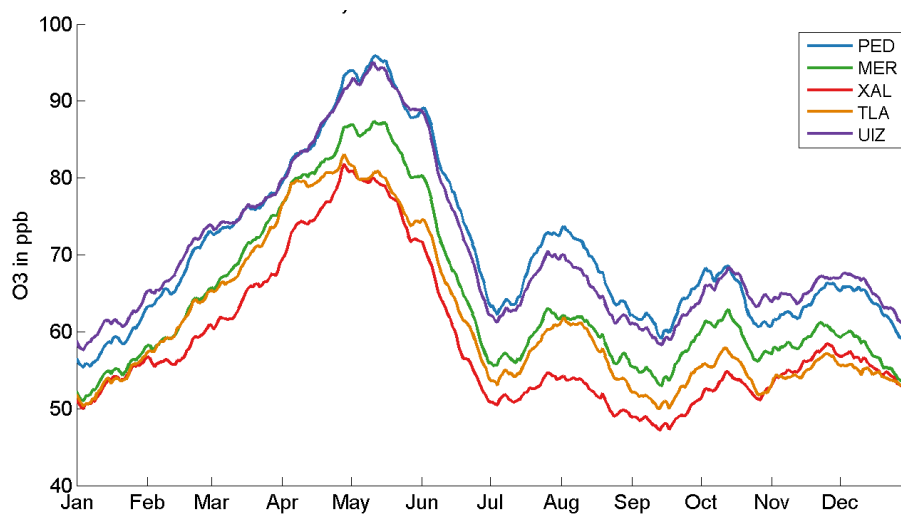
617

618 **Figure 1:** Locations of RAMA surface ozone stations used in this study (colored dots;
619 abbreviations defined in Table 1) and topographic height (shaded, in m) of the Mexico City
620 metropolitan region. State boundaries shown as black contours. Surface meteorology station at
621 Tacubaya (TCBY) also indicated. The inset in the upper right corner shows the location of
622 Mexico City within Mexico.



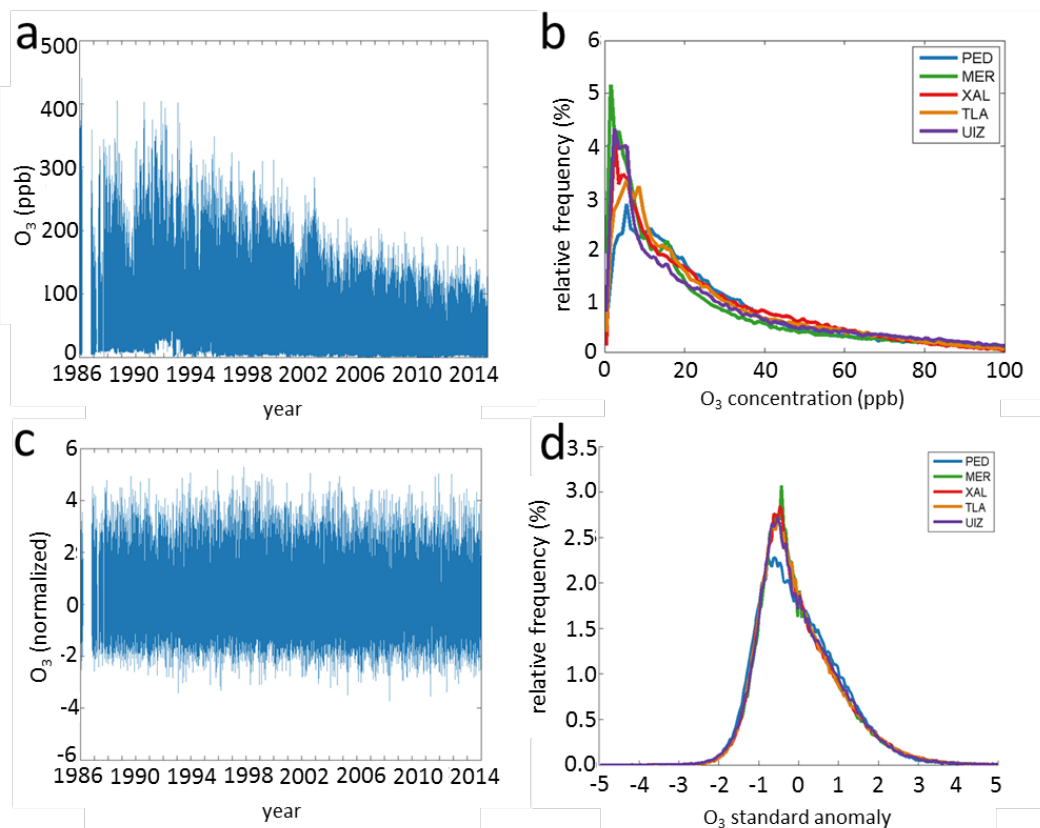
623

624 **Figure 2:** (a) Diurnal cycle of surface ozone concentrations (ppb) at five observing stations
625 (colored lines), as well as the mean (black dotted line) for all seasons, 1986-2014. (b) Diurnal
626 cycle of surface ozone concentrations for Pedregal (PED; blue lines) and Xalostoc (XAL; red
627 lines) by season from the RAMA network, 1986-2014.



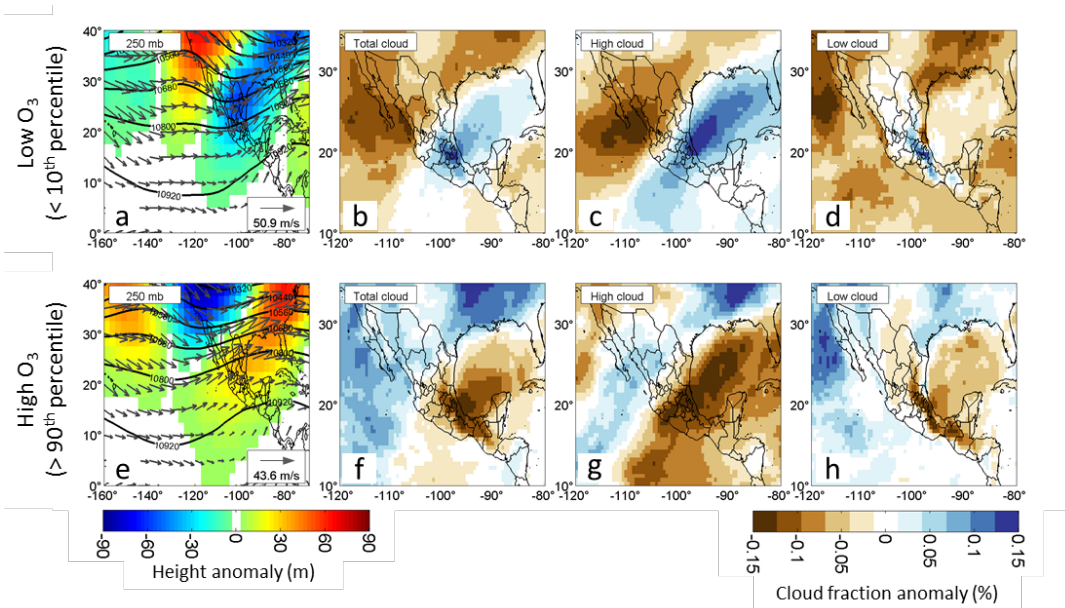
628

629 **Figure 3:** Annual cycles of surface ozone concentrations (ppb) for five observing stations for
630 hours 1200-1600 (local time) from the RAMA network, 1986-2014. Observations are smoothed
631 using a 30-day running mean.



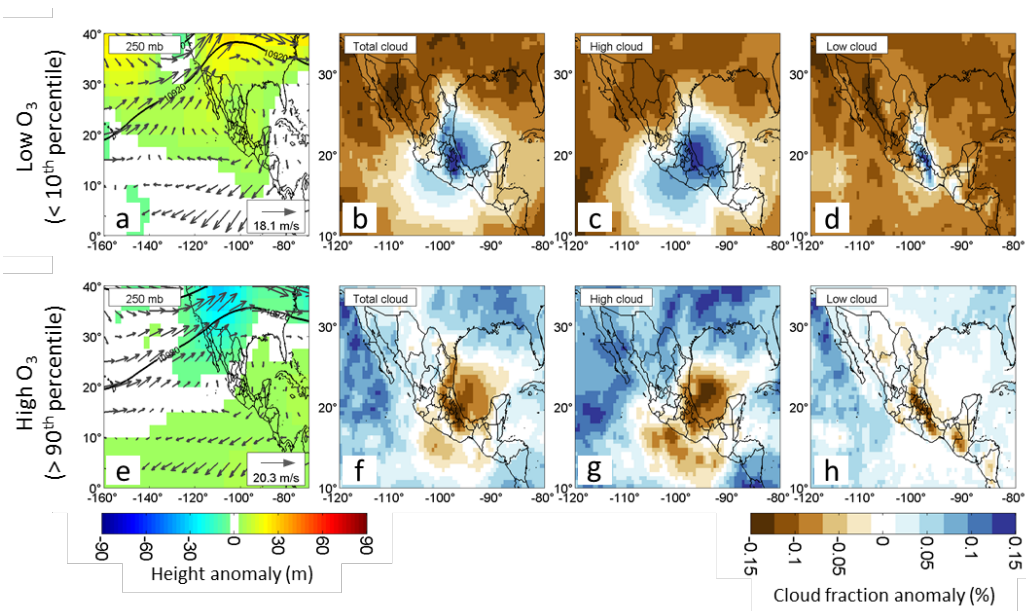
632

633 **Figure 4:** (a) Hourly observations of surface ozone concentrations (ppb) at Pedregal station
634 (PED in Fig. 1). (b) Relative frequencies (in %) of hourly ozone concentrations (ppb) at five
635 observing stations, 1986-2014. (c) Standard anomalies of hourly surface ozone concentrations at
636 PED. (d) Relative frequencies (in %) of standard anomalies of hourly ozone concentrations at
637 five observing stations from the RAMA network, 1986-2014.



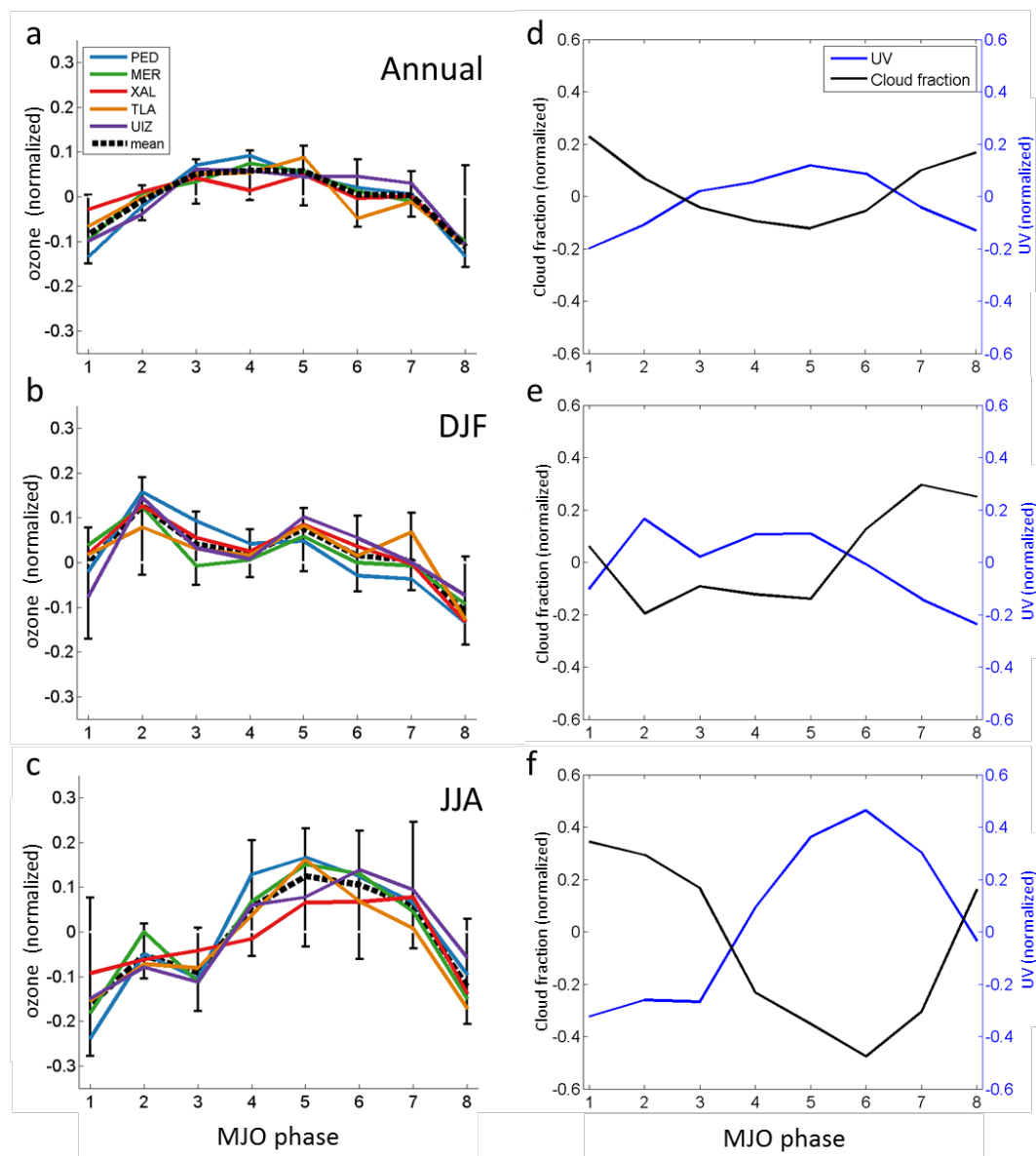
638

639 **Figure 5:** (a) Height (contoured, in m), height anomalies (shaded, in m), and mean winds
640 (vectors) at 250-hPa for winter (DJF) days with standard anomalies of afternoon (1200 to 1600
641 local time) surface ozone at the five observing stations (Fig. 1) below the 10th percentile. (b)-(d)
642 Anomalies (in %) of total cloud fraction, high cloud fraction, and low cloud fraction,
643 respectively, for the same winter days with standard anomalies of afternoon surface ozone
644 concentrations below the 10th percentile. (e)-(h) Same as in (a)-(d), but for winter days with
645 mean afternoon surface ozone concentrations above the 90th percentile. Percentile calculations
646 based on hourly observations from 1986-2014. Maximum wind speed (in m s^{-1}) is given in
647 lower-right corner of (a) and (e). Height, wind, and cloud fraction data are from ERA-Interim
648 reanalysis.



649

650 **Figure 6:** As in Figure 5, but for summer (JJA) days.



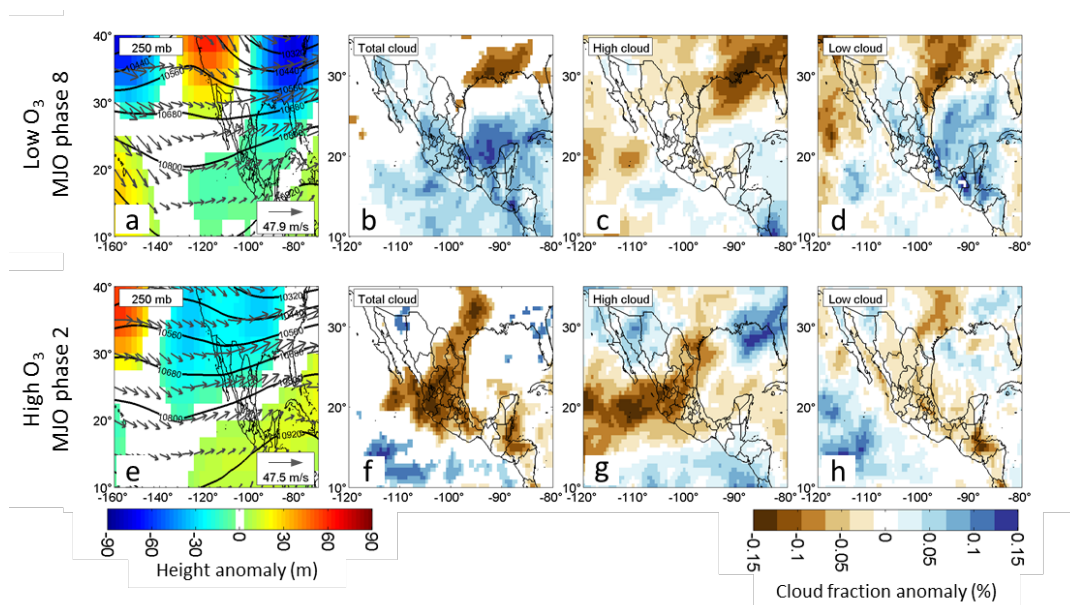
651

652 **Figure 7:** Mean standard anomalies of midday (hours 12-16 local time) surface ozone
 653 concentrations by active MJO phase for (a) annual, (b) DJF, and (c) JJA. Stations indicated by
 654 line color. Error bars indicate largest and smallest standard anomaly values for all stations;
 655 dashed black curves in (a)-(c) indicate mean values of all 5 observing stations. All surface ozone



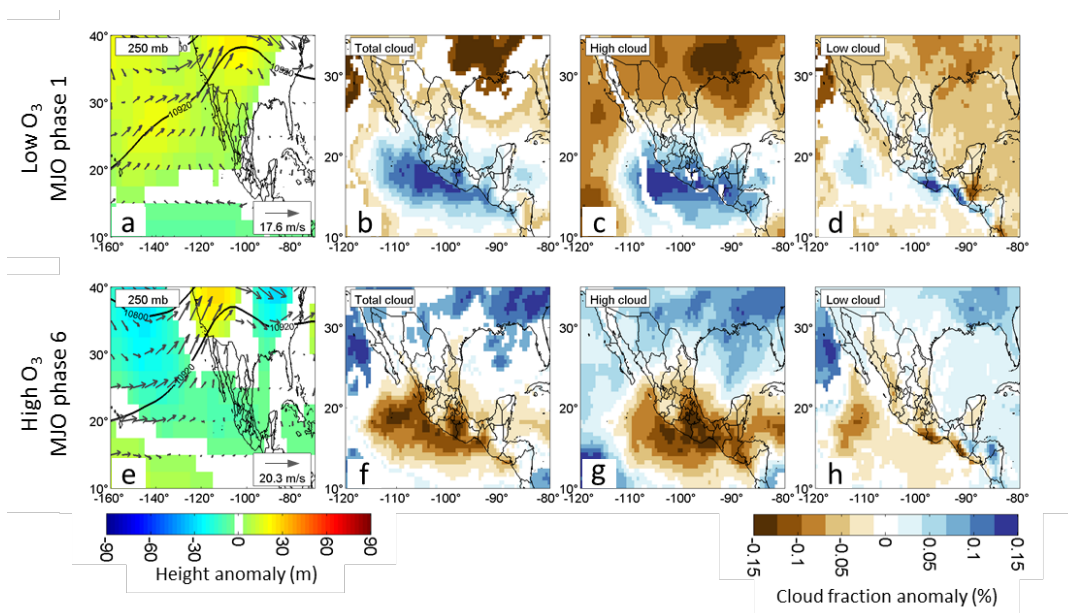
656 observations from the RAMA network, 1986-2014. (d) Standard anomalies of UV radiation (blue
657 curves) and total cloud fraction (black curves) for each active MJO phase for the entire year. (e)
658 and (f): same as panel (d) but for DJF and JJA, respectively. UV and cloud fraction data from
659 ERA-Interim reanalysis, 1986-2014, for the grid closest to Mexico City.

660



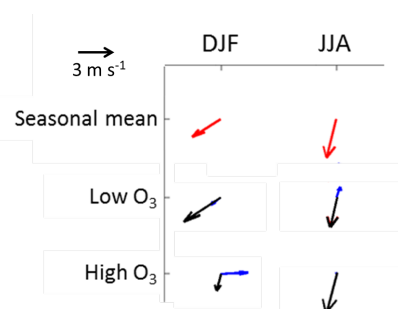
661

662 **Figure 8:** Composites of 250-hPa height (in m), height anomaly (in m), and mean wind (a), and
663 total cloud fraction (in %; b), high cloud fraction (in %; c), and low cloud fraction (in %; d) for
664 winter days in active MJO phase 8. (e)-(h) Same as (a)-(d) but for winter days in active MJO
665 phase 2. Maximum wind speed (in m s^{-1}) is given in lower-right corner of (a) and (e). Phases 8
666 and 2 were the phases with lowest and highest respective winter ozone concentrations in Mexico
667 City. Height, wind, and cloud fraction data are from ERA-Interim reanalysis.



668

669 **Figure 9:** As in Figure 8, but for summer days in active MJO phase 1 (a-d) and active MJO
670 phase 6 (e-h). Phases 1 and 6 were the phases with lowest and highest respective summer ozone
671 concentrations in Mexico City.



672

673 **Figure 10:** Mean 10-m winds at Tacubaya station (TCBY in Fig. 1) at 1800 UTC (1200 local
674 time). Mean surface wind vectors for each season, DJF and JJA, are on row one and indicated by
675 red arrows. Mean (black arrows) and anomaly (blue arrows) vectors for the MJO phases
676 associated with lowest surface ozone (phase 8 in DJF and phase 1 in JJA) are on the middle row.
677 Mean (black arrows) and anomaly (blue arrows) vectors for the MJO phases associated with
678 highest surface ozone (phase 2 in DJF and phase 6 in JJA) are on the bottom row. Note that the
679 mean winds for low ozone in DJF and high ozone in JJA are very similar to the seasonal mean
680 winds, so the anomaly (blue) vector is very small. All wind data are from NOAA National
681 Centers from Environmental Information, 1986-2014.